Journal of Sound and Vibration (1998) **216**(4), 623–636
Article No. sv981717

DYNAMIC STABILITY OF A FREE–FREE TIMOSHENKO BEAM SUBJECTED TO A PULSATING FOLLOWER FORCE

J.-H. KIM
Department of Aerospace Engineering, *Seoul National University*, 151–742, *Korea*

AND

Y.-S. CHOO
Agency for Defense Development, *P.O. Box* 35-4 *Yuseong Taejon* 305–600, *Korea*

(*Received* 23 *September* 1997, *and in final form* 30 *March* 1998)

The dynamic stability of a free–free Timoshenko beam with a concentrated mass is analyzed when a pulsating follower force $P_0 + P_1 \cos \Omega t$ is applied. The discretized equation of motion is obtained by the finite element method, and then the method of multiple scales is adopted to investigate the dynamic instability region. The effects of axial location and translation inertia of the concentrated mass are studied. The change of combination resonance types due to P_0, the relationship between critical forces and widths of instability regions in the vicinity of $2\omega_1$ (twice the first natural frequency of the bending vibration), and the effect of shear deformation are also examined.

1. INTRODUCTION

In general, forces acting on a structure can be divided into conservative forces and non-conservative forces. The follower force is a typical example of non-conservative forces. When a structure is under a constant follower force whose direction changes according to the deformation of the structure, it may undergo static instability (divergence) whereby transverse natural frequencies merge into zero, and dynamic instability (flutter), where two natural frequencies coincide with each other resulting in the amplitude of vibration growing without bound. Examples of structures subjected to constant follower forces include missiles, rockets and space vehicles changing orbit under thrust.

As is well known, the free–free beam serves as a simple model for missiles or rockets, and the thrust control machine can be thought of as a concentrated mass attached to the beam. The stability of free–free beams under constant follower forces has been studied in many papers [1–5]. Main results reported in those papers include the stability characteristics of the beam under controlled or pulsating follower forces [1], the effects of gain and location of control sensors, and the influences of rotary inertia and shear [2, 3]. In particular, Park [4] and Park and Mote Jr. [5] examined the maximum follower force of a free–free beam carrying

0022–460X/98/390623 + 14 $30.00/0

a concentrated mass. They predicted the location and magnitude of the mass that maximizes the critical force. Also, Sugiyama *et al*. [6] investigated the dynamic stability of a cantilevered column under a rocket thrust by regarding the rocket motor as a rigid body with a finite size (not as a point mass), and presented both theoretical and experimental results verifying the importance of magnitude and size of the concentrated mass.

On the other hand, Higuchi and Dowell [7, 8] examined the instability phenomena of a completely free edged plate by modal analysis, neglecting the rotary inertia and shear deformation due to constant follower forces. It was shown that critical forces are sensitive to the variation of aspect and Poisson ratios.

When a beam or a plate is exposed to an axial or in-plane pulsating force not greater than a critical value, they respectively experience an axial or in-plane vibration only. However, if certain conditions are satisfied between driving frequency and transverse natural frequency, then dynamic instability called ''parametric resonance'' occurs and the amplitude of transverse vibration increases without bound. This kind of instability was studied in references [9–12] for a beam under axial pulsating thrusts with focus placed on the effects of boundary conditions, longitudinal resonance, spring characteristics and slenderness ratio, etc. Recently Kar and Sujata [13] dealt with a rotating cantilever beam with an end mass under a transverse follower parametric excitation. The extended Galerkin method was utilized together with the method of multiple scales to investigate the influences of system parameters. Cederbaum and Mond [14] examined the relationship between stability and viscoelasticity of a viscoelastic column whose behavior is characterized by the Boltzmann superposition principle. Lee [15] treated an inextensible beam and analyzed how initial curvature and tip mass affect the dynamic instability.

Existing results reveal that pulsating forces also have an effect on the stability of aerospace structures. Young and Chen [16, 17] studied a cantilevered skew plate on which aerodynamic and harmonic in-plane forces act simultaneously. In references [18–20] a laminated composite plate with periodic loads was analyzed with respect to lamination scheme, lamination angle, boundary conditions, stiffening scheme and thickness, etc.

To the authors' knowledge, no literature except [1] has been concerned with the stability of a free–free beam under a pulsating follower force. This paper discusses the stability of a free–free Timoshenko beam carrying a concentrated mass under a pulsating follower force. The discretized equation of motion is obtained by the finite element method, and then the method of multiple scales is adopted to investigate the dynamic instability region. Numerical results are presented to demonstrate how the instability region changes according to parameters, such as the location and transverse inertia of the concentrated mass, and the shear deformation.

2. THEORY

A simple beam with length L is shown in Figure 1. A pulsating follower force $P_0 + P_1 \cos \Omega t$ is applied to the beam at an angle $\psi(L, t)$ with respect to the x-axis

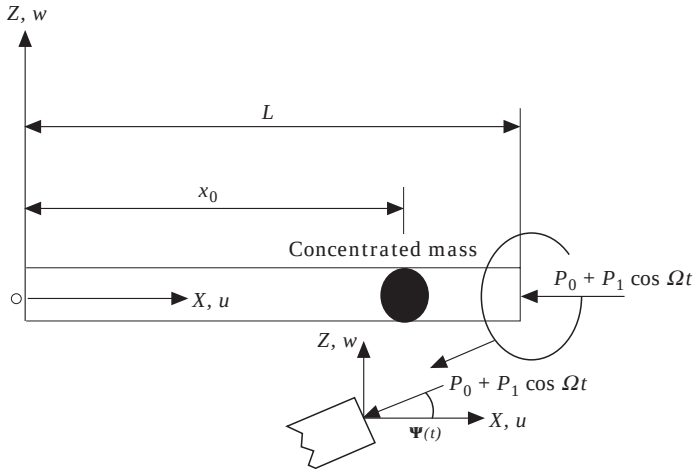

Figure 1. Free-free Timoshenko beam model subjected to pulsating follower force.

for an undeformed beam, where P_0 and P_1 are the magnitudes of constant and time-varying forces, respectively, and Ω is the driving frequency. A concentrated mass is attached at x_0.

2.1. ENERGY EQUATION AND EXTERNAL WORK

Let $\psi(x, t)$ and $w(x, t)$ respectively denote the rotation in the x-z plane and the deflection parallel to the z-axis of the beam. Then the displacement fields with account taken of shear deformation are given by

$$u_1(x, y, z, t) = -z\psi(x, t), \qquad u_2(x, y, z, t) = 0, \qquad u_3(x, y, z, t) = w(x, t), \quad (1)$$

where u_1, u_2, u_3 are interpreted as the displacements of an arbitrary point (x, y, z) along the x-, y- and z- axes, respectively. Note that the displacement of the neutral axis is neglected in (1). For the displacement fields given in (1), the strain energy U is given by

$$U = \tfrac{1}{2} \int_V \tau_{ij}\epsilon_{ij} \, \mathrm{d}V = \tfrac{1}{2} \int_0^L [EI\psi_{,x}^2 + kAG(w_{,x} - \psi)^2] \, \mathrm{d}x, \quad (2)$$

where EI denotes the bending stiffness and kAG the shear stiffness. On the other hand, the total kinetic energy T of the beam model can be computed by summing the kinetic energies of the beam itself and the concentrated mass as [5]:

$$T = \tfrac{1}{2} \int_V \rho \dot{u}_i \dot{u}_i \, \mathrm{d}V + \tfrac{1}{2} M w(x_0, t)_{,t}^2 + \tfrac{1}{2} J \psi(x_0, t)_{,t}^2$$

$$= \tfrac{1}{2} \int_0^L [\rho A w_{,t}^2 + \rho I \psi_{,t}^2] \, \mathrm{d}x + \tfrac{1}{2} M w(x_0, t)_{,t}^2 + \tfrac{1}{2} J \psi(x_0, t)_{,t}^2 \quad (3)$$

where ρA is the mass per unit length, ρI is the inertia per unit length, M and J are the translation and rotary inertia of the concentrated mass respectively.

The compressive axial force varies linearly along the axis for a beam with uniformly distributed material. However, the additional inertia force effect should be considered if a concentrated mass is attached. As a result, the axial force is distributed according to the function [5]

$$\hat{P}(x) = [\rho A x + M\mathrm{H}(x - x_0)]/[\rho A L + M](P_0 + P_1 \cos \Omega t), \tag{4}$$

where H is the Heaviside function. Also, the external works W_c and δW_{nc} done by axial and vertical components of the follower force are described as follows:

$$W_c = \tfrac{1}{2}\int_0^L \hat{P}(x) w_{,x}^2 \, \mathrm{d}x, \qquad \delta W_{nc} = -(P_0 + P_1 \cos \Omega t)\psi(L, t)\delta w(L, t). \tag{5, 6}$$

2.2. FORMULATION

For the system described in Section 2.1, Hamilton's principle can be expressed by

$$\delta \int_{t_1}^{t_2} (T - U + W_c) \, \mathrm{d}t + \int_{t_1}^{t_2} \delta W_{nc} \, \mathrm{d}t = 0. \tag{7}$$

To discretize the equation of motion induced by Hamilton's principle, one uses three-node Lagrange beam elements, as follows:

$$w = \sum_{i=1}^{3} h_i w_i, \qquad \psi = \sum_{i=1}^{3} h_i \theta_i, \tag{8}$$

where h_i denotes the shape function which is described in reference [24].

Applying Hamilton's principle and the finite element method, one obtains the following equation of motion:

$$\mathrm{M}\{\ddot{u}\} + [\mathrm{K}_e - \alpha P_{cr}\mathrm{K}_{g_s}]\{\mathbf{u}\} - [\beta P_{cr}\mathrm{K}_{g_t} \cos \Omega t]\{\mathbf{u}\} = 0, \tag{9}$$

where $\alpha = P_0/P_{cr}$, $\beta = P_1/P_{cr}$, P_{cr} is critical load, $\{\mathbf{u}\}$ is the n-dimensional vector of the beam, M is the mass matrix, K_e is the bending stiffness matrix, K_{g_s} and K_{g_t} respectively denote the geometric stiffness matrices due to constant and time-varying follower forces. If, as in this paper, constant and time-varying forces are applied in the same way, then one has $\mathrm{K}_g = \mathrm{K}_{g_s} = \mathrm{K}_{g_t}$. Let $\mathrm{K} = \mathrm{K}_e - \alpha P_{cr}\mathrm{K}_g$ and rewrite equation (9) as

$$\mathrm{M}\{\ddot{\mathbf{u}}\} + \mathrm{K}\{\mathbf{u}\} - \beta P_{cr} \cos \Omega t \mathrm{K}_{g_t}\{\mathbf{u}\} = 0. \tag{10}$$

Note that K is an unsymmetrical matrix due to the non-conservative force.

M and K are now transformed into diagonal matrices using modal transformation. In general, one rigid body translation mode and one rigid body rotation mode appear for a free–free beam. To exclude the effect of rigid body modes, modal vectors related to only elastic vibration modes are used in the

transformation. Let $\mathbf{\Phi}$ and $\mathbf{\Psi}$ be the $n \times (n-2)$ normalized right and left modal matrices respectively. Substituting the transformation $\{\mathbf{u}\} = \mathbf{\Phi}\{\boldsymbol{\eta}\}$ and premultiplying by $\mathbf{\Psi}^{\mathrm{T}}$ on both sides, equation (10) leads to the following equation of motion:

$$\mathbf{I}\{\ddot{\boldsymbol{\eta}}\} + \mathbf{\Lambda}\{\boldsymbol{\eta}\} - \beta P_{cr} \cos \Omega t \mathbf{R}\{\boldsymbol{\eta}\} = 0 \tag{11}$$

with $\mathbf{\Psi}^{\mathrm{T}}\mathbf{M}\mathbf{\Phi} = \mathbf{I}$, $\mathbf{\Psi}^{\mathrm{T}}\mathbf{K}\mathbf{\Phi} = \mathbf{\Lambda}$, $\mathbf{\Psi}^{\mathrm{T}}\mathbf{K}_g\mathbf{\Phi} = \mathbf{R}$ and $\mathbf{I}$ the identity matrix. Note that the diagonal entries of $\mathbf{\Lambda}$ are just the squares, w_i^2, $1 \leqslant i \leqslant n-2$, of the natural frequencies of the beam under a constant follower force. Rewriting (11) in component form, one has

$$\ddot{\eta}_j + w_j^2 \eta_j + [2\epsilon \cos \Omega t] \sum_{m=1}^{n-2} \tilde{R}_{jm} \eta_m = 0, \qquad j = 1, 2, \ldots, n-2, \tag{12}$$

where $\epsilon = -\beta/2$ and $\tilde{R}_{jm} = R_{jm} P_{cr}$. According to the method of multiple scales, the solutions of (12) can be expressed by a series expansion of ϵ as follows [23]:

$$\eta_j(t, \epsilon) = \sum_{m=0}^{\infty} \epsilon^m \eta_{jm}(T_0, T_1, T_2, \ldots), \qquad j = 1, 2, \ldots, n-2, \tag{13}$$

where $T_n = \epsilon^n t$, $n = 0, 1, 2, \ldots$.

Through the first order approximation, i.e., by considering the first two terms only in (13), one can define transition curves that separate stable solutions from unstable ones in the $\epsilon - \Omega$ plane by (see [23] for details)

(a) $\Omega \simeq \omega_p + \omega_q$ (sum type combination resonance)

$$\Omega = \omega_p + \omega_q \pm \epsilon[\tilde{R}_{pq}\tilde{R}_{qp}/\omega_p\omega_q]^{1/2} + \mathcal{O}(\epsilon^2), \tag{14.1}$$

(b) $\Omega \simeq \omega_q - \omega_p$ (difference type combination resonance)

$$\Omega = \omega_q - \omega_p \pm \epsilon[\tilde{R}_{pq}\tilde{R}_{qp}/-\omega_p\omega_q]^{1/2} + \mathcal{O}(\epsilon^2). \tag{14.2}$$

From (14.1) and (14.2), it is easily seen that the sum type and difference type combination resonances cannot exist simultaneously for any pair of natural frequencies ω_p and ω_q. Furthermore, if a force is of a constant direction type, then the difference type combination resonance does not appear due to the symmetry of $\mathbf{R}$. For a follower force, however, $\tilde{R}_{pq}$ and $\tilde{R}_{qp}$ can have opposite signs, and so the difference type may also exist.

3. NUMERICAL RESULTS AND DISCUSSION

For analyzing the dynamic stability, non-dimensional parameters are defined as: $\bar{\Omega} = [\Omega^2 \rho A L^4/EI]^{1/2}$ (driving frequency), $\bar{\omega}_i = [\omega_i^2 \rho A L^4/EI]^{1/2}$ (natural frequency), $\bar{P}_{cr} = P_{cr}L^2/EI$ (critical force), $S = kAGL^2/EI$ (shear deformation parameter), $R = I/AL^2$ (rotary inertia parameter of beam), $\bar{M} = M/\rho AL$ (mass ratio between concentrated mass and beam), $\bar{J} = J/\rho AL^3$ (rotary inertia parameter of concentrated mass), $\mu = x_0/L$ (axial location of concentrated mass from non-thrusting end).

TABLE 1

Comparison of critical force

	$S = 10^6$			$S = 10^3$		
	$\bar{M} = 0$	$\bar{M} = 0{\cdot}2$, $\bar{J} = 0$	$\bar{M} = 0{\cdot}2$, $\bar{J} = 10^{-3}$	$\bar{M} = 0$	$\bar{M} = 0{\cdot}2$, $\bar{J} = 0$	$\bar{M} = 0{\cdot}2$, $\bar{J} = 10^{-3}$
Present	111·4	181·6	177·9	102·4	161·1	159·4
Reference [5]	111·5	186·5	181·6	102·6	160·9	159·9
Reference [4]	109·6	178·6	–	–	–	–

First, the validity of the code used in the present numerical calculations is checked. To this end the critical forces generated by the code with those of references [4] and [5] is compared, for the case where the beam divided into 20 elements and is under a constant follower force. Comparison results are summarized in Table 1. In the case of $S = 10^3$, the critical forces of the code differ only by 0·3% or so from those of [5]. When $S = 10^6$ and a concentrated mass is considered, 2·6% in maximum difference is observed. On the other hand, approximately 1·7% differences exist between the present code and [4] when the free–free beam is considered as an Euler–Bernoulli beam (note that the effects of rotary inertia and shear deformation rarely appear when $S = 10^6$). These comparison results indicate the validity of the code using 20 Lagrange elements.

3.1. EFFECTS OF SHEAR DEFORMATION AND P_0 MAGNITUDE

Perturbation theories, including the method of multiple scales, are based on the assumption that some coefficients of terms are sufficiently small [23]. Figure 2 compares the first and second order approximations of solutions given in (13). The

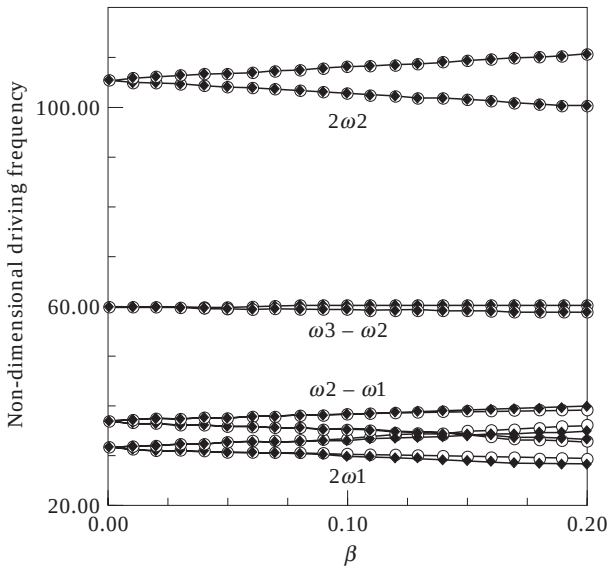

Figure 2. Comparison of 1st expansion and 2nd expansion solutions ($S = 10^6$, $R = 0$, $\alpha = 0{\cdot}4$).

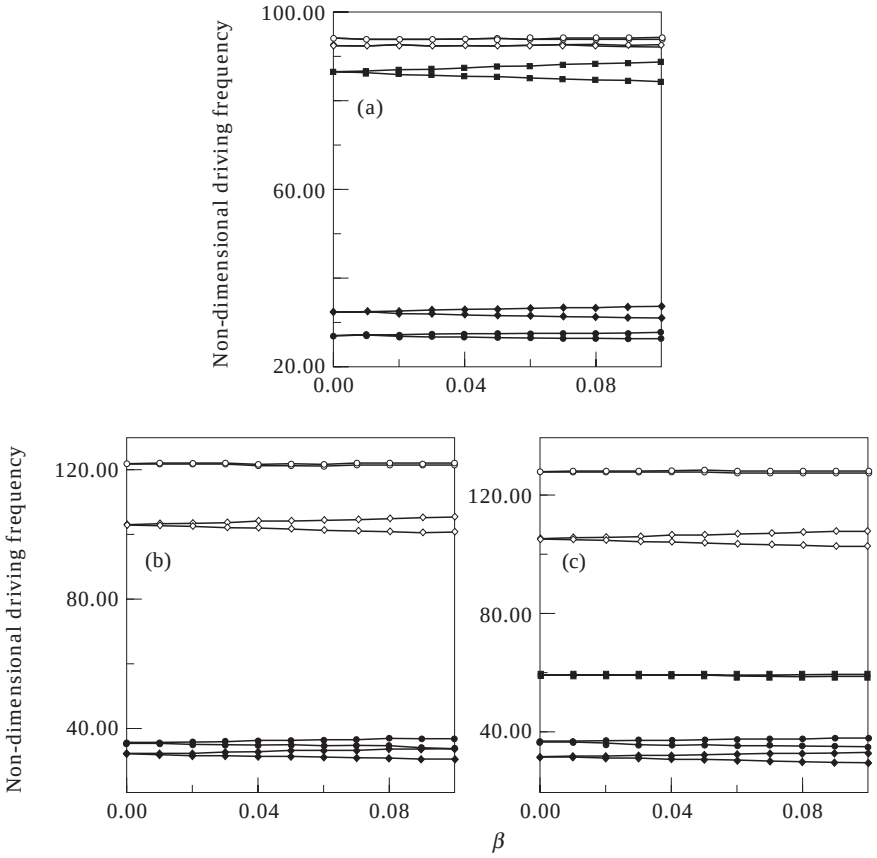

Figure 3. Parametric instability region of beam without a concentrated mass, (a) $S = 10^2$; (b) $S = 10^3$; (c) $S = 10^6$ ($R = 0$, $\alpha = 0{\cdot}4$).

expressions for transition curves for the latter case can be found in [23]. Solutions of the type $\Omega = \omega_q \pm \omega_p$ are chosen to determine the range of β for the numerical calculation. From the figure it is easily seen that, for $0 \leqslant \beta \leqslant 0{\cdot}1$, transition curves for the first and second order approximations show no big difference. Furthermore the two curves almost coincide with each other in the region corresponding to relatively higher frequencies. As a result, one may restrict numerical studies to the region $0 \leqslant \beta \leqslant 0{\cdot}1$ and can ensure the accuracy of results concerning the dynamic instability obtained by using the first order approximation.

Dynamic instability regions for $S = 10^2$, 10^3 and 10^6 are plotted in Figure 3. And the first four non-dimensional natural frequencies and the critical force for each case are listed in Table 2. Instability regions due to the combination of different modes appear around $\omega_2 - \omega_1$ and $\omega_3 + \omega_1$ in all cases. Other instability regions are observed near $\omega_4 - \omega_1$ and $\omega_3 - \omega_2$ for $S = 10^2$ and 10^6 respectively. Note that the regions around $2\omega_1$, $2\omega_2$ and $\omega_2 - \omega_1$ have relatively larger widths than the others. Such effects of shear deformation are shown in Figure 4 in detail. Since stability boundary curves expressed by the first order approximation are

TABLE 2

Non-dimensional natural frequencies and critical forces ($R = 0$)

S	$\bar{\omega}_1$	$\bar{\omega}_2$	$\bar{\omega}_3$	$\bar{\omega}_4$	$\bar{P}_{cr}$
10^2	16·15	43·15	76·11	109·93	61·6
10^3	16·00	51·33	105·76	174·54	102·4
10^6	15·93	52·84	112·74	193·81	111·4

linear, one can compute the variation of an instability region using the following equation [19]:

$$\bar{R}_{ij} = \hat{R}_{ij}/\hat{R}_s[\bar{\Omega}_s^2/\bar{\Omega}_i\bar{\Omega}_j]^{0\cdot5} \tag{15}$$

where $\hat{R}_s$ and $\bar{\Omega}_s$ are reference values. The term "slope ratio" indicates $\bar{R}_{ij}$, i.e., the ratio of width between reference instability region and other instability regions. The result reveals that the effect of shear deformation becomes remarkable for $S = 10^3$ and less, from which one can conclude that shear deformation reduces the widths of instability regions.

Figure 5 shows the influence of P_0 on the dynamic instability for the same values of S. The width near $2\omega_1$ for $\alpha = 0{\cdot}1$ is used as a reference in the figure. An abrupt increase of the instability region can be seen as P_0 approaches the critical force. This indicates that the larger the mean external force P_0 is, the more unstable the structure becomes. For small α, combination resonance occurs in the sum type $\omega_3 + \omega_1$. However, it is replaced by the difference type $\omega_3 - \omega_1$ for large α. In Figures 5(a) and (c) the transition points are $\alpha = 0{\cdot}44$ and $0{\cdot}62$ respectively, which

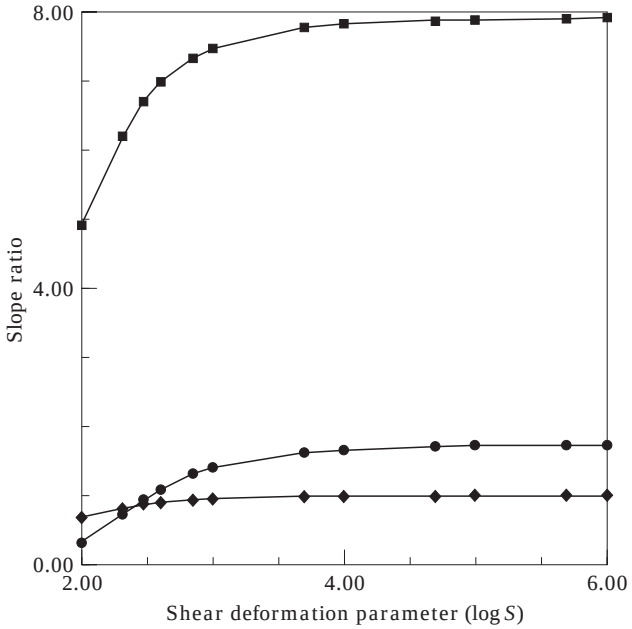

Figure 4. Effect of shear deformation ($R = 0$, $\alpha = 0{\cdot}4$).

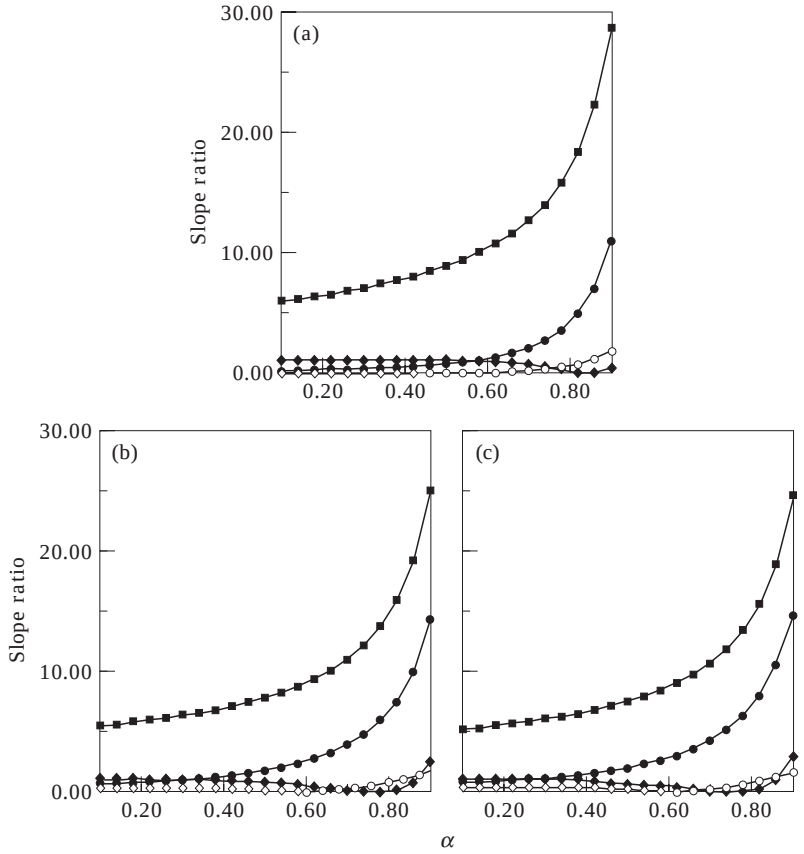

Figure 5. Effect of a on parametric instability region of beam without a concentrated mass, (a) $S = 10^2$; (b) $S = 10^3$; (c) $S = 10^6$ ($R = 0$).

implies that the transition occurs at smaller α as S decreases, i.e., as the effect of shear deformation increases. Investigating the width of the instability region near $2\omega_1$, one can see that it initially decreases and then increases from some value of α. In Figure 6, the first non-dimensional natural frequency curve ($\bar{\omega}_1$) under constant follower force is shown. Note that in both figures the curves start to increase from the same value of α. This phenomenon appears when critical forces are of the flutter type, and can also be observed in section 3.2.

3.2. EFFECT OF A CONCENTRATED MASS

In Figure 7 the effect of the location of the concentrated mass on dynamic instability for the case $\bar{M} = 0{\cdot}2$ is shown. The first four non-dimensional natural frequencies and the critical force for each case are listed in Table 3. An instability region appears around $\omega_2 - \omega_1$ regardless of the location of the mass. On the other hand, other types of combination resonances are very sensitive to the location of the concentrated mass. While combination resonances occur in the form of $\omega_3 + \omega_1$ and $\omega_3 - \omega_2$ for $\mu = 0{\cdot}3$, they change to the types $\omega_3 - \omega_1$ and $\omega_3 + \omega_2$ when $\mu = 0{\cdot}5$. In the case of $\mu = 0{\cdot}6$, only difference type combination resonance

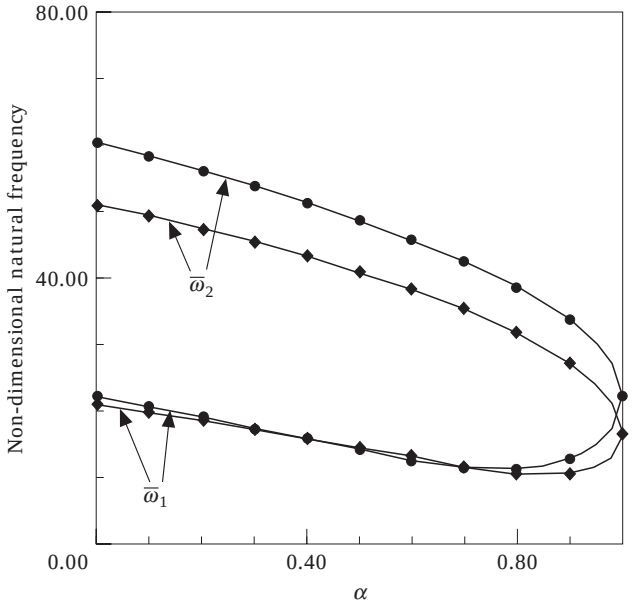

Figure 6. Eigenvalue curve of a beam subjected to a constant follower force without a concentrated mass ($R = 0$).

appears except near $2\omega_1$. The plots for $\mu = 0{\cdot}7$ and $0{\cdot}9$ show that combination resonance of the sum type replaces that of the difference type as μ increases.

Figure 8 shows how the width and type of instability region change according to α and μ. The reference is the slope of the instability region near $2\omega_1$ for $\alpha = 0{\cdot}1$. When $\mu = 0{\cdot}3$, the type of combination resonances changes from $\omega_3 - \omega_2$ and $\omega_3 + \omega_1$ to $\omega_3 + \omega_2$ and $\omega_3 - \omega_1$ respectively. However, for $\mu = 0{\cdot}5$, instability regions, except near $2\omega_1$, become wider without any change in combination resonance types. At $\mu = 0{\cdot}7$, the instability region near $\omega_3 + \omega_1$ increases according to α, and then decreases from $\alpha = 0{\cdot}68$. Note that this point does not coincide with the point from which the instability region near $2\omega_1$ starts to increase. When $\mu = 0{\cdot}9$, the combination resonance type changes from $\omega_3 + \omega_1$ to $\omega_3 - \omega_1$. The entire instability region increases abruptly in the case of $\mu = 0{\cdot}5$, and becomes less sensitive to α when the concentrated mass is located near the end point. Comparing

TABLE 3

Non-dimensional natural frequencies and critical forces ($S = 10^3$, $R = 0{\cdot}00032$, $\bar{M} = 0{\cdot}2, \bar{J} = 0$)

μ	$\bar{\omega}_1$	$\bar{\omega}_2$	$\bar{\omega}_3$	$\bar{\omega}_4$	$\bar{P}_{cr}$
0·3	18·93	49·34	104·09	172·34	89·8
0·5	18·20	55·77	95·94	174·53	88·3
0·6	18·59	52·49	104·34	157·02	104·6
0·7	18·43	48·53	103·08	168·40	159·0
0·9	18·26	55·88	109·64	172·16	79·6

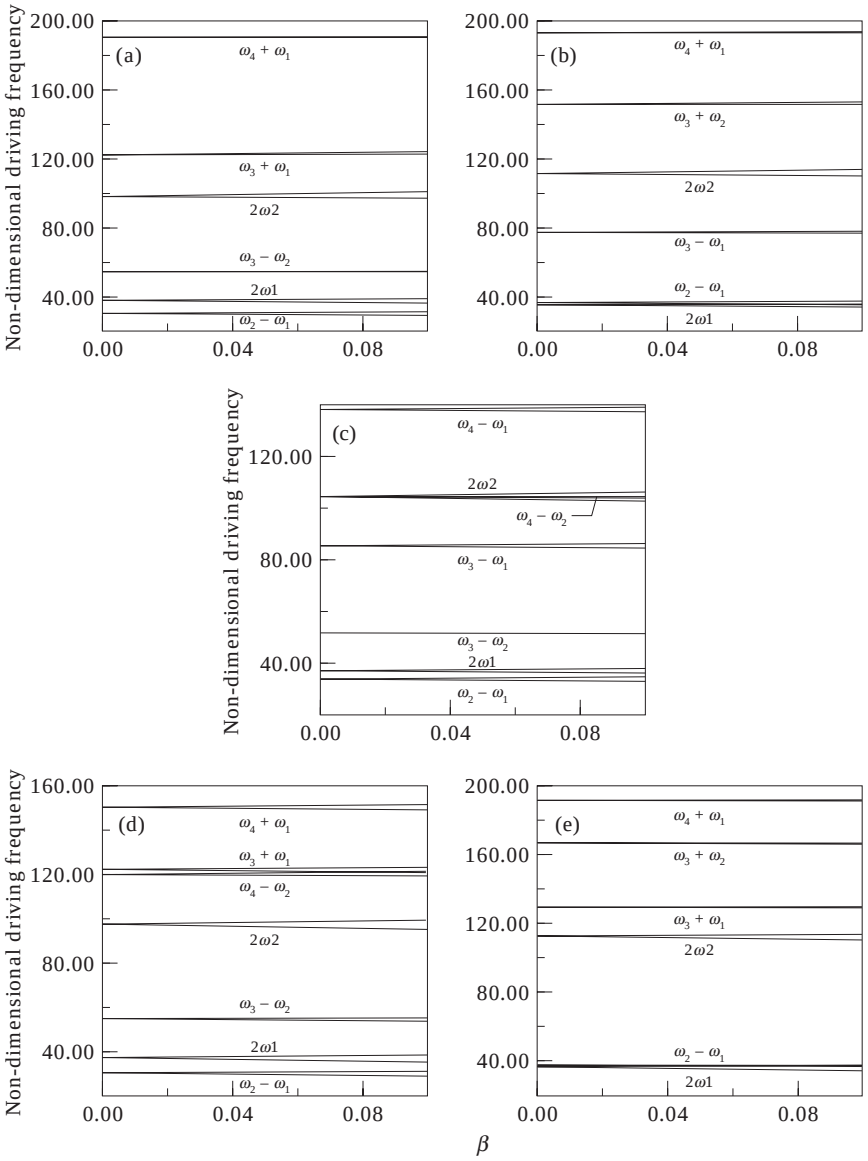

Figure 7. Parametric instability regions of beam with a concentrated mass, (a) $\mu = 0{\cdot}3$; (b) $\mu = 0{\cdot}5$; (c) $\mu = 0{\cdot}6$; (d) $\mu = 0{\cdot}7$; (e) $\mu = 0{\cdot}9$ ($S = 10^3$, $R = 0{\cdot}00032$, $\bar{M} = 0{\cdot}2$, $\bar{J} = 0$, $\alpha = 0{\cdot}2$).

the results for $\mu = 0{\cdot}3$ and $0{\cdot}7$, one can see that the instability region undergoes less change as the concentrated mass approaches the thrusting end rather than the non-thrusting end. The case where $\mu = 0{\cdot}9$ shows a different tendency from others in that the instability region keeps increasing in size. As mentioned in section 3.1, this is related to the type of critical force. Namely, as can be seen from Figures 8(a)–(c), the instability region near $2\omega_1$ and curve of $\bar{\omega}_1$ simultaneously start to increase from the same value of α when the critical force is of the flutter type. The curve of $\bar{\omega}_1$ does not appear here. However, the critical force is of the

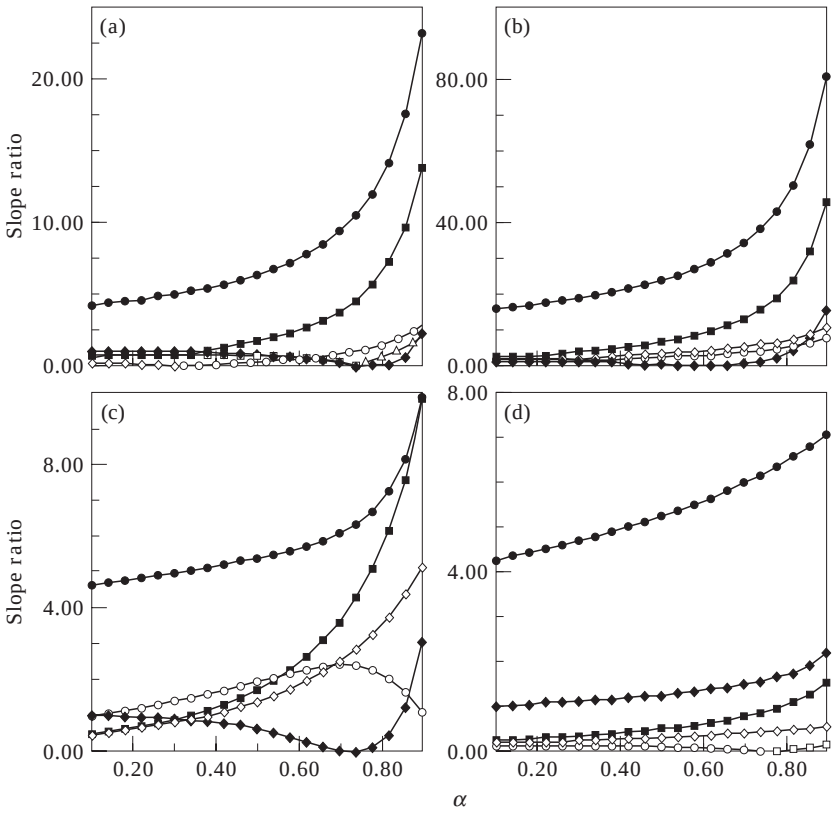

Figure 8. Effect of a on parametric instability region of beam with a concentrated mass, (a) $\mu = 0{\cdot}3$; (b) $\mu = 0{\cdot}5$; (c) $\mu = 0{\cdot}7$; (d) $\mu = 0{\cdot}9$ ($S = 10^3$, $R = 0{\cdot}00032$, $\bar{M} = 0{\cdot}2$, $\bar{J} = 0$).

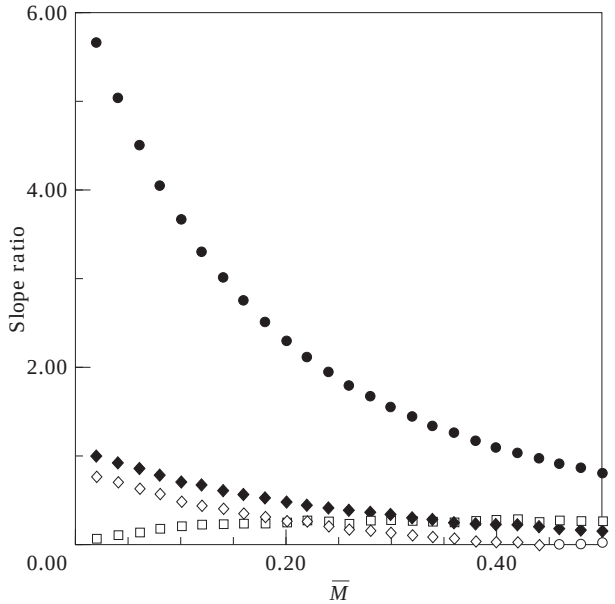

Figure 9. Effect of translational inertia of a concentrated mass, ($S = 10^3$, $R = 0{\cdot}00032$, $\mu = 0{\cdot}7$, $\bar{J} = 0$, $\alpha = 0{\cdot}2$).

divergence type for $\mu = 0{\cdot}9$ and so the instability region around $2\omega_1$ continues to increase in this case.

Figure 9 describes the effect of the translational inertia of the concentrated mass. The reference is the slope of the instability region near $2\omega_1$ when a thrust corresponding to $\alpha = 0{\cdot}2$ at $\bar{m} = 0{\cdot}02$ is applied. It is easily seen that the larger the translation inertia of the concentrated mass, the smaller the instability region. In other words, the system becomes more stable as the mass ratio between the concentrated mass and beam increases. Also, the increase of $\bar{M}$ alters the combination type from $\omega_2 - \omega_1$ to $\omega_2 + \omega_1$.

4. CONCLUSIONS

In this paper the dynamic stability of a free–free Timoshenko beam with a concentrated mass for a pulsating follower force $P_0 + P_1 \cos \Omega t$ has been studied. The discretized equation of motion was obtained by the finite element method, and then the method of multiple scales was used to investigate the dynamic instability region.

The conclusions obtained in the paper can be summarized as:

(1) The variation of the instability region near $2\omega_1$ is closely related to the type of critical force. When the critical force is of the flutter type, the instability region initially decreases and then starts to increase from some value of P_0. However, the region increases monotonically according to P_0 for a divergence-type critical force.

(2) Some of the combination resonances change from sum type to difference or vice versa as P_0 increases.

(3) Combination resonances related to higher modes are very sensitive to the location of the concentrated mass. For example, difference type combination resonances are dominant for $\mu = 0{\cdot}6$, but sum type combination resonances appear remarkably for $\mu = 0{\cdot}9$.

(4) The translational inertia of the concentrated mass enhances the stability by reducing the instability region.

(5) Shear deformation decreases the instability region and changes the types of combination resonances.

ACKNOWLEDGMENT

The authors thank the Korea Science and Engineering Foundation (KOSEF) for financial support via the research project No. 961-1002-017-2.

REFERENCES

1. T. R. Beal 1965 *American Institute of Aeronautics and Astronautics Journal* **3**, 486–494. Dynamic stability of a flexible missile under constant and pulsating thrusts.
2. J. J. Wu 1976 *Journal of Sound and Vibration* **49**, 141–147. On missile stability.
3. Y. P. Park 1987 *Journal of Sound and Vibration* **113**, 407–415. Dynamic stability of a free Timoshenko beam under a controlled follower force.

4. Y. P. Park and C. D. Mote Jr. 1985 *Journal of Sound and Vibration* **98**, 247–256. The maximum controlled follower force on a free–free beam carrying a concentrated mass.
5. Y. P. Park and B. J. Ryu 1987 *Proceedings of the KSME/JSME Vibration Conference* 309–318. Effect of a concentrated mass on the stability of a free Timoshenko beam under a controlled follower force.
6. Y. Sugiyama, J. Matsyike, B. A. Ryu, K. Katayama, S. Kinoi and N. Enomoto 1995 *American Institute of Aeronautics and Astronautics Journal* **33**, 499–503. Effect of concentrated mass on stability of cantilevers under rocket thrust.
7. K. Higuchi and E. H. Dowell 1990 *American Institute of Aeronautics and Astronautics Journal* **28**, 1300–1305. Dynamic stability of a rectangular plates with four free edges subjected to a follower force.
8. K. Higuchi and E. H. Dowell 1989 *Journal of Sound and Vibration* **129**, 255–269. Effects of the Poisson ratio and negative thrust of the dynamic stability of a free plates subjected to a follower force.
9. J. E. Brown, J. M. Hutt and A. E. Salama 1968 *American Intitute of Aeronautics and Astronautics Journal* **6**, 1423–1425. Finite element solution to dynamic stability of bars.
10. J. S. Huang and L. H. Hung 1984 *International Journal for Non-linear Mechanics* **19**, 287–301. Dynamic stability for a simply supported beam under periodic axial excitation.
11. B. P. Shastry and G. V. Rao 1984 *Computers and Structures* **19**, 823–827. Dynamic stability of bars considering shear deformation and rotary inertia.
12. S. K. Sinha 1989 *Journal of Sound and Vibration* **131**, 509–514. Dynamic stability of a Timoshenko beam subjected to an oscillating axial force.
13. R. C. Kar and T. Sujata 1992 *Journal of Sound and Vibration* **154**, 81–93. Stability boundaries of a rotating cantilever beam with end mass under a transverse follower excitation.
14. G. Cederbaum and M. Mond 1992 *Journal of Applied Mechanics* **59**, 16–19. Stability properties of a viscoelastic column under a periodic force.
15. H. P. Lee 1995 *International Journal for Solids Structures* **32**, 3377–3392. Effects of initial curvature on the dynamic stability of a beam with tip mass subjected to axial pulsating loads.
16. T. H. Young and F. Y. Chen 1994 *Journal of Sound and Vibration* **171**, 603–615. Stability of skew plates subjected to aerodynamic and in-plane forces.
17. T. H. Young and F. Y. Chen 1993 *American Institute of Aeronautics and Astronautics Journal* **31**, 1667–1673. Stability of fluttered panels subjected to in-plane harmonic forces.
18. R. S. Srinivasa 1986 *Computer and Structures* **24**, 233–238. Dynamic stability of rectangular laminated composite plates.
19. G. Cederbaum 1991 *American Institute of Aeronautics and Astronautics Journal* **29**, 2000–2005. Dynamic instability of shear deformable laminated plates.
20. C. L. Liao and C. R. Cheng 1994 *Journal of Sound and Vibration* **174**, 335–351. Dynamic stability of stiffened laminated composite plates and shells subjected to in-plane pulsating forces.
21. H. Ziegler 1968 *Principles of Structural Stability*. Waltham, MA: Blaisdell Publishing.
22. V. V. Bolotin 1964 *The Dynamic Stability of Elastic Systems*. San Francisco, CA: Holden-Day.
23. A. H. Nayfeh and D. T. Mook 1979 *Nonlinear Oscillations*. New York: John Wiley.
24. G. Dhatt and G. Touzot 1984 *The Finite Element Method Displayed*. New York: John Wiley.